

The COVID-19 Pandemic from the Eye of the Virus

Faryad Darabi Sahneh¹, William Fries², Joseph C. Watkins^{1,2,3,4},
Joceline Lega^{1,3,4,*}

¹ Department of Mathematics, University of Arizona,

² Interdisciplinary Program in Applied Mathematics, University of Arizona,

³ Department of Epidemiology and Biostatistics, University of Arizona,

⁴ BIO5 Institute, University of Arizona,
Tucson, AZ, 85721 USA

*To whom correspondence should be addressed; E-mail: lega@math.arizona.edu.

Abstract

The all-pervasive lens that humans ordinarily use to watch and analyze the pandemic is *time*. This article considers an alternative. Instead of tracking incidence as a function of time, new cases are counted as a function of *cumulative cases*. This resource-centric perspective, which is more natural and physically justified, is the perspective of the virus. In this article, we demonstrate the relevance of this approach by characterizing an outbreak as an independent increments Gaussian process that fluctuates about a deterministic curve, called the incidence-cumulative cases (ICC) curve. We illustrate these concepts on Influenza A and COVID-19 outbreaks in the US. The novel perspective presented here reveals universal properties of disease spread that would otherwise remain hidden.

As evidenced by the COVID-19 pandemic, societies throughout the world are highly vulnerable to disease outbreaks [1]. Understanding disease transmission is therefore crucial to timely and effective public health policies. To this end, scientists have developed numerous mathematical, statistical, and computational models of infectious disease dynamics [2]. But because disease spread is inherently complex, such descriptions often rely on large numbers of parameters that may be difficult to estimate. Any effort that reduces model complexity while maintaining core features is therefore invaluable.

In most instances, the independent variable underlying the course of an epidemic is time: health authorities report numbers of new cases and deaths per day or week, forming what is commonly called an epidemiological (EPI) curve (see examples in the top left panel of Figure 1); and modelers fit their models to this same EPI curve. However, time – as

we measure it – is not intrinsic to virus spread dynamics. As such, we argue that when focusing on temporal aspects of virus spread, many modeling and inference efforts obscure relevant properties of the dynamics, thereby making it more difficult to fit models to data.

Dynamical systems theory has long promoted a “phase portrait” perspective that can provide both intuitive insights and analytical approaches not easily identified under the normal time domain description. Expanding on the viewpoint fostered in [3, 4] to apply such a perspective to outbreak analysis, this article reveals how simple universal structures emerge from microscopic stochastic interactions. It also offers a more refined and streamlined analysis of important statistical properties of single disease outbreaks.

Outbreaks beyond the time domain

Finding an alternative domain to analyze epidemics begins by considering the reachable available resources for the pathogen. From this standpoint, susceptible hosts are the resources. At each point in time, all that matters for a pathogen is what resources are available for further invasion or, equivalently if infectivity is high, what resources have been used. As illustrated in Figure 1, this point of view offers valuable insight on important traits shared by different outbreaks associated with the same pathogen. The left plot of the top row shows the EPI curves of the 24 Influenza A (H3N2) outbreaks that took place in US HHS regions between 1998 and 2019 and led to more than 3000 confirmed cases. No specific properties of these curves are readily observable, because the peak timing and peak height vary between seasons. However, when the same curves are plotted in the incidence vs. cumulative cases (ICC) plane, a structure emerges, revealing similarities between each season that, as we will see, are characteristic of the disease itself. To emphasize that such properties are generic, the bottom row of Figure 1 shows similar results for multiple instances of the spread of a disease on a network, as described by a stochastic SIR (Susceptible, Infected, Recovered) model. Again, the universality normally hidden behind classical EPI curves becomes evident once time is removed from the picture and the independent variable is replaced with cumulative cases.

In the deterministic compartmental SIR model, the total number of cases is $C = I + R$, and the total population $n = S - C$ is fixed. It was shown in [4] that knowledge of $C(t)$ is equivalent to knowledge of $S(t)$, $I(t)$, and $R(t)$, and that the SIR dynamics can be recast as an autonomous differential equation of the form $\bar{\mathcal{I}} = dC/dt = nG(C/n)$, where $\bar{\mathcal{I}}$ is the deterministic incidence, C is the cumulative number of cases, and G is a function of C that depends on the parameters of the outbreak.

The relevance of the SIR model to COVID-19 outbreaks is illustrated in Figure 2, which shows daily incidence in the state of Arizona for the 2020 calendar year, both in the time domain (top row: standard EPI curve) and in the cumulative cases domain (bottom row: ICC curve). The first arrow marks the end of the initial stay at home period (03/19/2020 - 05/15/2020) ordered by the Governor of Arizona [5, 6, 7]; the second arrow, on August

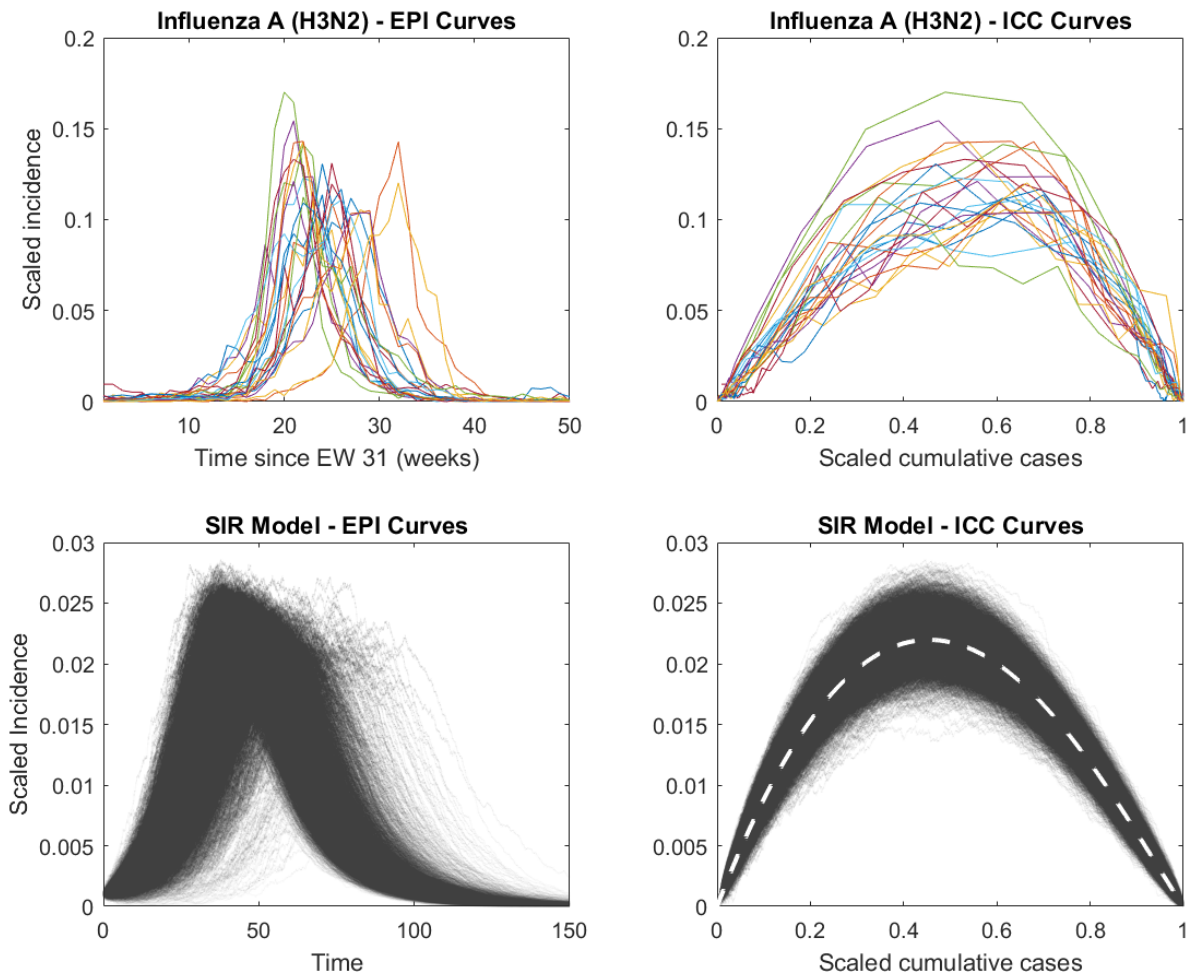


Figure 1: **Top Row, left:** weekly incidence $\mathcal{I}/\hat{C}_\infty$ plotted as a function of time, for influenza A (H3N2) outbreaks that took place in the US between 1998 and 2019, and were of final size $\hat{C}_\infty > 3000$ cases. Each curve corresponds to one flu season in an HHS region. Time is measured in weeks from epidemiological week (EW) 31 of each year. The data were downloaded from the CDC Fluview database using the R `cdcfluview` package [21]. **Top row, right:** the same curves plotted in the ICC plane, showing $\mathcal{I}/\hat{C}_\infty$ as a function of scaled cumulative cases C/\hat{C}_∞ . **Bottom row, left:** EPI curves for 5997 runs of a stochastic SIR model with size $N = 2500$ and $R_0 = 2$. **Bottom row, right:** Corresponding ICC curves, showing $\mathcal{I}/\hat{C}_\infty$ as a function of C/\hat{C}_∞ . The white dashed curve corresponds to Equation 1, scaled to the expected final size C_∞ of the outbreak (C_∞/N is the non-zero root of the right-hand side of Eq. 1 with c_0 set to 0.).

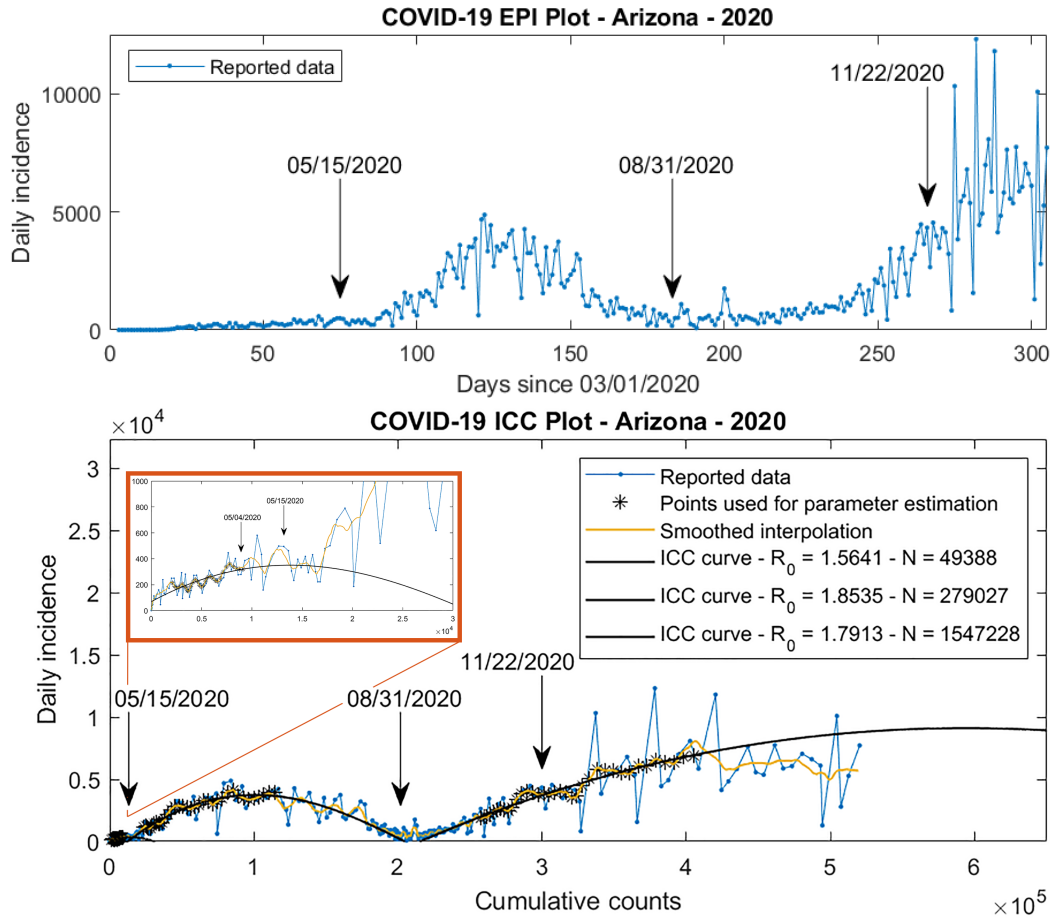


Figure 2: COVID-19 outbreak in the state of Arizona in 2020, from March 1st to December 31st. **Top:** Daily incidence as a function of time. **Bottom:** Daily incidence as a function of cumulative cases. The inset magnifies the region with less than 30,000 cumulative cases. The three waves are well approximated by ICC curves for the SIR model (black solid lines), whose parameters were found using a range (stars) of smoothed incidence values (yellow). The nonlinear relationship between cumulative counts C and time is reflected by the change in spacing between the arrows in the top and bottom plots. COVID-19 case data provided by The COVID Tracking Project at *The Atlantic* under a CC BY-NC-4.0 license [22].

31st, indicates the end of the first six months of the outbreak (the first two cases were reported in Arizona on 03/04/2020); the third arrow marks the last day the number of cumulative cases in the state was below 300,000. Whereas the spacing between consecutive dates (108 and 83 days respectively) is similar in the time domain (top plot), this is no longer true in the cumulative case domain (bottom plot), which reveals that about twice as many cases were reported between 05/15/2020 and 08/31/2020 than between 08/31/2020 and 11/22/2020. The inset displays an enlargement of the ICC curve for the first 30,000 cases (in the time domain, from 03/04/2020 to 06/10/2020). The first arrow corresponds to 05/04/2020, when it was announced that the stay at home order would end [8, 9] before 05/15/2020 (second arrow). Three different waves are visible in the bottom plot, each of which is locally well approximated by an ICC curve (in black) of the form $\bar{I} = N G(c)$, where $c = C/N$, $c_0 = C_0/N$, and

$$G(c) = \beta_P \left(c + \frac{1}{R_0} \ln(1 - c) - \frac{1}{R_0} \ln(1 - c_0) \right) (1 - c). \quad (1)$$

Here N is the effective populations size, β_P is the population contact rate of the disease, R_0 is the basic reproductive number, and C_0 represents initial conditions. Equation 1 is the exact relationship between incidence \bar{I} and cumulative cases C for the deterministic SIR model [4]. The parameters used to fit each wave vary, indicating an increase in the effective size N (estimated at 49,388 individuals for the first wave, 279,027 for the second, and 1,547,228 for the third) as the outbreak unfolds, while the basic reproduction number R_0 fluctuates between 1.5 and 2 (respective estimates are 1.56, 1.85, and 1.79). The corresponding values of β_P and $\gamma = \beta_P/R_0$ are $(\beta_P, \gamma) \simeq (0.12, 0.08)$, $(0.21, 0.11)$, and $(0.16, 0.09)$ respectively.

In what follows, we provide a quantitative description of the advantage ICC curves have over EPI curves when describing outbreaks.

In the cumulative case domain, temporal stochasticity factors out

Epidemics are commonly modeled using Markov processes [10]. In the case of the SIR model, the size of each compartment evolves according to a continuous time Markov process involving the two transitions described in Table 1. In the limit of large population n , the expected sizes of the S , I , and R compartments follow a system of differential equations (the deterministic SIR model) that describes the evolution of these mean-field variables. To analyze the system from the perspective of the virus, where time is not intrinsically essential, we can leverage the power of the Gillespie algorithm to separate temporal stochasticity from the evolution of the state $\mathcal{S} = (n_S, n_I, n_R)$ of the system. Indeed, the Gillespie algorithm shows that the SIR process may be decomposed into two parts: 1) (essential to the human perspective) the length of time that the process remains

event	transition	rate
infection	$(n_S, n_I, n_R) \rightarrow (n_S - 1, n_I + 1, n_R)$	$\beta n_S n_I$
recovery	$(n_S, n_I, n_R) \rightarrow (n_S, n_I - 1, n_R + 1)$	γn_I

Table 1: Continuous-time Markov process associated with the SIR model. Here, n_S is the number susceptible, n_I is the number infected, n_R is the number recovered, and β is the contact rate of the disease.

in its current state \mathcal{S} is exponentially distributed with parameter value depending only on \mathcal{S} through the rates given in Table 1; 2) (sufficient for the virus perspective) the jumps form an underlying time-homogeneous discrete time Markov chain. More importantly these two components are independent! (See e.g. [11], Section 15.6 and [12]).

Additionally, provided the number of infected individuals $n_I > 0$, the **cumulative number of cases** $n_C = n_I + n_R = n - n_S$ forms a time-homogeneous discrete time pure birth Markov chain:

$$n_C \rightarrow n_C + 1, \text{ with probability } \lambda(n_C), \quad (2)$$

where

$$\lambda(n_C) = \frac{\beta n_S n_I}{\beta n_S n_I + \gamma n_I} = \frac{\beta n_S}{\beta n_S + \gamma} = \frac{R_0(1 - n_C/n)}{R_0(1 - n_C/n) + 1},$$

and the **basic reproduction number** is the ratio $R_0 = n\beta/\gamma = \beta_P/\gamma$. The assumption that $n_I > 0$ is not restrictive for analyzing an outbreak while infection events happen. Decomposing a time continuous Markov process into a discrete time jump process whose events are separated by exponentially distributed time intervals is a common practice. What makes such a decomposition particularly useful here is that whereas the number of infections and recoveries depends on n_I (Table 1), the evolution of n_C (Equation 2) is self-contained: it only depends on the total population n and on the basic reproduction number R_0 . Since only a ratio of rates, R_0 , appears in the expression for $\lambda(n_C)$, it is clear that β (or equivalently β_P) is an ancillary parameter for the chain and, as a consequence, time does not explicitly appear in the model. This is also reflected in Equation 1, in which β_P factors out: the unit of time used to estimate incidence is implicitly defined through the parameter β_P .

The above formulation thus provides a twofold complexity reduction. First, the temporal stochasticity of time intervals between events is factored out. Second, individual outbreaks may be described in terms of a single variable n_C , instead of the usual two-dimensional description involving n_I and n_R . Moreover, n_C presents the advantage of increasing monotonically as the outbreak unfolds. As will be seen in the following, such a reduction preserves all the core information relevant to the epidemic process. Furthermore, the cumulative number of cases is what is directly available from public health reports.

The number of recovery events between fixed values of n_C is independent of the infected population size

In the pure birth Markov chain of Equation (2), a single infection event happens with probability $\lambda(n_C)$. Between two infection events, recoveries that do not change the cumulative case count take place each with probability $1 - \lambda(n_C)$. Hence, the number of recovery events that occur before a new infection takes place is a geometric random variable with parameter $\lambda(n_C)$. But, because $\lambda(n_C)$ only depends on n_C , the number of recovery events that occur while the cumulative number of cases goes from $n_{C_0} = c_0 n$ to $n_C = c n$ is the sum of $n_C - n_{C_0}$ independent $\lambda(m)$ geometric variables, $m = n_{C_0}, \dots, n_C - 1$, and is therefore independent of the number of infected individuals n_I at any point $n_{C'}$ (including $n_{C_0} < n_{C'} < n_C$) as long as $n_I > 0$. Similarly, since $n_C = n_I + n_R$, the change in the infected population size while cumulative cases increase from n_{C_0} to n_C is $n_I - n_{I_0} = (n_C - n_{C_0}) - (n_R(c) - n_R(c_0))$, which only depends on c and c_0 and is independent of n_{I_0} . Furthermore, the number of recoveries between n_{C_0} and n_C is independent of the number of recoveries between $n_{C'_0}$ and $n_{C'}$ whenever the intervals (C'_0, C') and (C_0, C) are not overlapping.

Additionally, we calculate the following mean and variance (see materials & methods for details):

$$E\left(\frac{n_R(c)}{n} - \frac{n_R(c_0)}{n}\right) \simeq \frac{1}{R_0} \ln\left(\frac{1 - c_0}{1 - c}\right),$$

$$n \text{Var}\left(\frac{n_R(c)}{n} - \frac{n_R(c_0)}{n}\right) \simeq \frac{1}{R_0} \ln\left(\frac{1 - c_0}{1 - c}\right) + \frac{1}{R_0^2} \frac{c - c_0}{(1 - c)(1 - c_0)},$$

with equality in the limit as $n \rightarrow \infty$. It may seem surprising that the above expectation and variance only depend on c and c_0 . Indeed, as discussed earlier, the overall epidemic process is expected to be a function of the susceptible population $n_S = n - n_C$ (the available resources) and the size of the infected population n_I (measuring the capability of a virus to annex additional resources), while recovery events only depend on the infection population. However, the above formulas indicate that n_I does not play any role. This is to be contrasted with the number of individuals who recover between time t_0 and t , which is typically modeled as a binomial random variable, with a mean and variance that are proportional to the number of infected.

To understand how the infected population size may not contribute to the number of recoveries that take place during a fixed increase in the number of cases, imagine two cities experiencing outbreaks with identical model parameters. Assume that, at a particular point in time, both cities have reported the same number of cumulative cases C_0 , but one of them, City A, has 50% more infectious people than the other city (City B). Then, over a fixed time interval, City A will, on average, have 50% more recoveries than City B. What the above formulas tell us is that over a fixed number ΔC of new cases

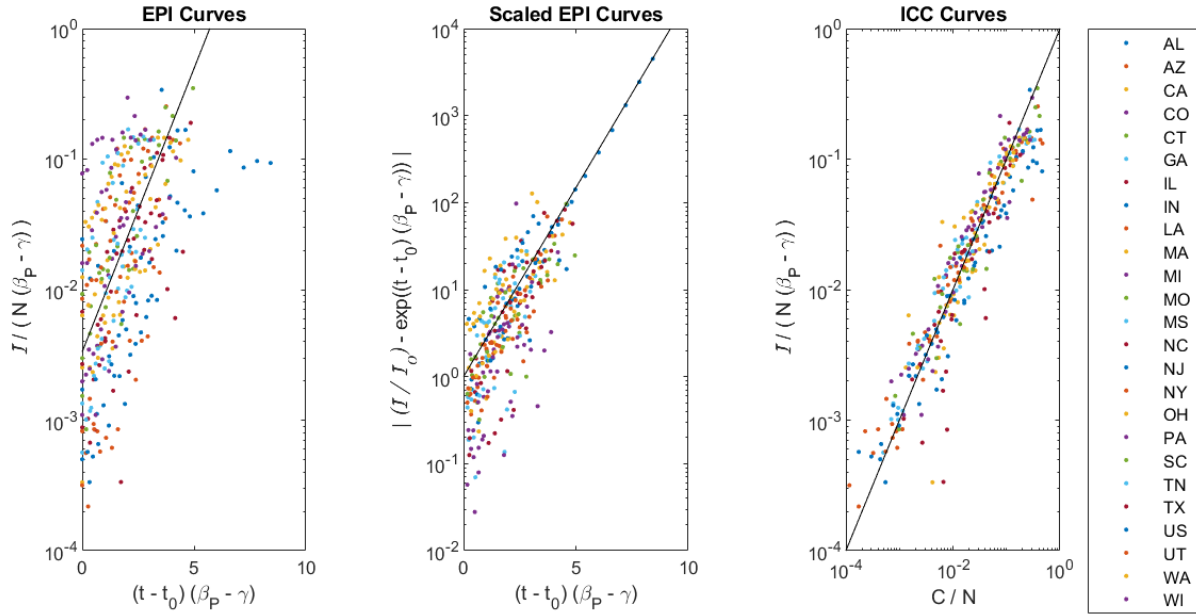


Figure 3: Early COVID-19 outbreaks in the US: all of the states that had at least 1000 cases by 04/01/2020 are included. **Left:** (EPI curves) lin-log plot of $\mathcal{I}/((\beta_P - \gamma)N)$ as a function of $\tau = (t - t_0)(\beta_P - \gamma)$, where t_0 is the time at which COVID-19 cases started to grow in the specified region. **Middle:** (Scaled EPI curves) lin-log plot of $|\mathcal{I}/\mathcal{I}_0 - \exp(\tau)|$ as a function of τ , where \mathcal{I}_0 is the incidence at $t = t_0$. **Right:** (ICC curves) log-log plot of $\mathcal{I}/((\beta_P - \gamma)N)$ as a function of C/N . In each panel, the black solid line represents the expected trend, corresponding to exponential growth in the left and middle panels, and to a linear relationship in the right panel. COVID-19 case data provided by The COVID Tracking Project at *The Atlantic* under a CC BY-NC-4.0 license [22].

however, the number of recoveries will have the same distribution in both cities. The reason is that City A will reach the higher level of cases ($C = C_0 + \Delta C$) faster than City B, and thus lessen the time for individuals to recover. This will occur in a way to exactly match the distribution of the number of recoveries in City B. Such a balance in cases and recoveries reduces the variance in the models and guides strategies for estimation that has both lower bias and variance.

Estimation errors do not accumulate in the cumulative case domain

The cumulative case domain is particularly useful for inference and forecasting, especially at the beginning of an outbreak. In realistic scenarios we only have records of incidence,

or equivalently, numbers of cumulative cases, and it is customary to look for an estimation of the size of the infectious population, either explicitly or implicitly. If we are estimating infection numbers in the time domain, errors in the estimation of the initial infection size grow exponentially with parameter $\beta_P - \gamma$. The standard deviation also grows exponentially, at the same rate (see [13] and note that $n_S \simeq n$ in the early stages of the outbreak). Thus, a small uncertainty in the number of infected n_I at the beginning of a prediction interval is exponentially amplified. As shown in the left and middle panels of Figure 3 for COVID-19 in the US, a similar behavior is observed for the incidence \mathcal{I} as a function of time. This is to be expected since, in the deterministic SIR model for instance, incidence is given by the product $\beta n_I n_S \simeq \beta_P n_I$ at the onset of an outbreak. Case reports in the US and in the states that had at least 1000 cases by 04/01/2020 were used to estimate regional values of the contact rate β_P , the recovery rate γ , and of the effective population size N , in order to plot the scaled incidence $\mathcal{I}/(N(\beta_P - \gamma))$ as a function of time (left panel) and of C/N (right panel). We use N instead of n here to emphasize that N is the empirically estimated value of n . An estimate of the standard deviation $|\mathcal{I}/\mathcal{I}_0 - \exp((t - t_0)(\beta_P - \gamma))| = \delta\mathcal{I}$ is shown in the middle panel. Both \mathcal{I} and $\delta\mathcal{I}$ grow exponentially in time (straight solid line in the left and middle panels; note the linear-log scale), confirming exponential amplification of uncertainty in the time domain. In contrast, the right panel of Figure 3 shows that $\mathcal{I}/(N(\beta_P - \gamma))$ is a *linear* function of C/N (note the log-log scale) and that much less dispersion is observed in the cumulative case domain. This is because increments in the C -domain are independent; as a consequence, the error in the number of infections at the beginning of a C interval does not affect the prediction of changes in the number of infected individuals in a subsequent interval. In addition, the variance is well controlled and decreases with increased values of R_0 . If we define incidence of the stochastic SIR model as $\mathcal{I} = \beta n_I n_S = \beta n_I (n - n_C)$, where n_I and n_S are random variables, we calculate that, in the limit of large n , the mean of $\mathcal{I}_n = \mathcal{I}/n$ evolves according to Equation 1 with $c_0 = 0$ as a function of $c = n_C/n$, and that the variance satisfies

$$\frac{1}{n} \text{Var}(\mathcal{I}) \rightarrow \beta_P^2 \left(-\frac{1}{R_0} \ln(1 - c) + \frac{1}{R_0^2} \frac{c}{(1 - c)} \right) (1 - c)^2$$

as $n \rightarrow \infty$, which again shows that $\text{Var}(\mathcal{I})$ is only a function of c (see materials & methods).

To summarize, while \mathcal{I} grows exponentially in the time domain at the beginning of an outbreak, it only grows linearly in the cumulative case domain. As a consequence, uncertainties on \mathcal{I} are amplified in the time domain, but not in the cumulative case domain. This is dramatically illustrated in the choice of scales for the axes in Figure 3.

R_0	$\mu_{\hat{c}_\infty} = c_\infty$	σ_∞	$\mu_{\hat{c}_\wedge} = c_\wedge$	σ_\wedge	c_\wedge/c_∞
1.2	0.314	3.708	0.152	0.434	0.485
1.5	0.583	1.835	0.273	0.448	0.468
2.0	0.797	0.913	0.363	0.386	0.455
2.5	0.893	0.547	0.403	0.335	0.452
3.0	0.941	0.357	0.426	0.297	0.453
3.5	0.966	0.245	0.440	0.268	0.455
4.0	0.980	0.174	0.450	0.246	0.459
4.5	0.988	0.126	0.457	0.229	0.462
5.0	0.993	0.094	0.462	0.214	0.465

Table 2: Values for the means of the fraction of population that eventually become cases $\mu_{\hat{c}_\infty} = c_\infty$, and the fraction of cases at peak infection $\mu_{\hat{c}_\wedge} = c_\wedge$. For a population of size n , the standard deviation for \hat{c}_∞ is σ_∞/\sqrt{n} . The standard deviation of \mathcal{I}/n at $c = c_\wedge$ is $(\beta n)\sigma_\wedge/\sqrt{n}$. The final column gives the ratio of means and shows the universality of the ICC curve over a range of values for R_0 .

In the cumulative case domain, peak incidence occurs at a universal fraction of the final size

We now investigate two circumstances of particular interest for an epidemic, namely the total number of infected individuals \hat{c}_∞ and the number of cases \hat{c}_\wedge at peak incidence. First, we write the relationship of the ICC curve as a differential equation $\frac{dc}{dt} = G(c)$, where $G(c)$ is given by Equation 1 with $c_0 = 0$. The mean final size $c_\infty = \mu_{\hat{c}_\infty}$ occurs when $G(c_\infty) = 0$, and the mean peak incidence $c_\wedge = \mu_{\hat{c}_\wedge}$ satisfies $G'(c_\wedge) = 0$. Because the parameter $\beta = \beta_P/n$ appears as a multiplicative factor in $G(c)$, the quantities c_∞ and c_\wedge do not depend on β , for R_0 and n fixed. Additional analytical properties may be obtained by employing the delta method (see materials & methods and [14], Section 11.4.), a combination of the central limit theorem and propagation of error. In particular, such an approach guarantees that the bias in the mean is small even for moderate size populations and that the distribution about the mean is normal with an explicitly stated variance (see Table 2). The result for the estimator \hat{c}_∞ has been known for several decades [15, 16, 17]. However, the distribution of the number of cases around mean peak incidence is seemingly new. These values are summarized in Table 2. Not surprisingly, the final size of the outbreak, c_∞ , increases with R_0 . Similarly, the value of c at peak incidence, c_\wedge , increases with R_0 . Notably, their ratio c_\wedge/c_∞ is nearly stable at 0.45 to 0.48 over a large range of values for R_0 , reflecting the universal properties of the shape of the ICC curve.

Discussion

The ICC curve [3, 4] ushers in a fundamentally new way of thinking about epidemics, both in its ability to convey a timely visual message to the public, and through a shift in perspective. It equips us with more powerful approaches to understand epidemic dynamics, to explore and evaluate policy decisions, and to ascertain quickly the impact of such decisions.

This article proposes implementing a shift from the human time-centric perspective (in terms of EPI curves) to the virus resource-centric perspective (in terms of ICC curves), thereby isolating ancillary parameters from the statistical analysis of single outbreaks. Specifically, we have developed a methodological framework (see materials & methods) allowing us to analyze a single outbreak as a stochastic process (describing incidence as a function of the number of cases) that fluctuates about a deterministic ICC curve with universal properties (Figure 1). For large populations, such an outbreak evolves according to a Gaussian process with independent increments, of mean given by the deterministic ICC curve (Figure 2). Furthermore, we have established explicit formulae for the limiting variance and skewness in the cumulative case domain (see materials & methods), where uncertainty is less amplified than in the time domain (Figure 3).

Remarkably, the underlying Markov chain for the discrete Markov SIR process is a pure birth chain in the number of cases, provided that there are some infected individuals in the population. The advantages of such a case-based approach are manifold, and are direct consequences of the analyses presented in this manuscript and its the materials & methods section. In particular, the Markov chain and its limit have a single parameter R_0 , and the contact rate β_P for infections is an ancillary parameter (see [18] for the properties of ancillary statistics). Consequently, for large populations, the independent increment nature of the Gaussian process factorizes likelihoods into a product of normal densities, thereby replacing time-series analysis with a weighted nonlinear regression for parameter estimation. Fisher information can be computed explicitly to give confidence regions for model parameters, in contrast to computationally intensive simulation-based approaches. Normal priors on the parameters are conjugate to the likelihood function in the cumulative case domain, which substantially simplifies any Bayesian analysis, as opposed to the typical MCMC methods used in the time domain. Importantly, the property of independent increments guarantees that estimates do not depend on the past history of the epidemic. This is dramatically illustrated in the three ICC curves that describe the course of COVID-19 in Arizona (Figure 2). Estimates of R_0 and N are entirely informed by the case-incidence data on only the portion of the epidemic under a given ICC curve. Data associated to the other two ICC curves cannot play any role.

Furthermore, our proposed approach can address recent challenges raised in the literature regarding time-based analysis of epidemics. Recently, Juul *et al.* [19] reported on the issues associated with fixed time statistics and the underestimation of extremes in epidemic curve ensembles. We noted before that whereas uncertainty is exponentially

amplified in the time domain, incidence rates grow linearly in the cumulative case domain. Moreover, the stochastic ICC process has independent increments and thus obviates the issues of long-term correlations. ICC curves therefore circumvent many of the shortcomings of fixed time statistics. In addition, the present approach provides an explicit strategy to compute confidence intervals for important epidemic events. Finally, the call for “curve based” statistics made in [19] is integral to the characterization of the epidemic as a realization of a Gaussian process. This allows us to incorporate the entire ICC curve in the likelihood associated with any estimation, including parameter inference, detecting the impact of changes for instance in behavior or due to the introduction of a vaccine, and in forecasting.

Of course, epidemics do not exactly follow an SIR model. The ICC curves, as seen from the ensemble of curves for H3N2 Influenza A outbreaks (Figure 1), or in the successive waves of COVID-19 (Figure 2), show that the SIR model is a compelling first approximation. A follow-up goodness of fit analysis will provide evidence into departures from this model. Of particular interest is how heterogeneous contact networks, a protracted asymptomatic period, or differential susceptibility and recovery times result in ICC curves that depart from Equation 1. These questions can be explored quickly using, for example, simulation approaches relying fundamentally on the analytical results articulated in this paper.

With a change of perspective from the human to the pathogen, this article shows that the nearly-century old Kermack-McKendrick [20] mathematical model is again the foundation for modern, even more powerful, analytical tools that yield clearer insights into the nature of an outbreak.

Acknowledgements

We are grateful to Mohammad Javad Latifi Jebelli for insightful conversations about this work.

Funding

FDS and JL acknowledge support from the National Science Foundation (DMS-2028401) RAPID grant. JCW acknowledges support from the National Science Foundation (CCF-1740858) TRIPODS Grant.

Author contributions

FDS and JL conceived of the project. JCW led in deriving the mathematical results. JL and WF coordinated the simulations and numerical results and generated figures. All authors contributed to the writing of the manuscript and approved the final version.

Competing interests

All authors declare that they have no competing interests.

Materials & Methods

Continuous Time Stochastic SIR Model

We consider a SIR epidemic model on a network. Nodes of the network represent individuals, and edges are connections between them. There is no spatial component in this model, and the architecture of the network remains unchanged during simulations. Disease spread is simulated with the Gillespie algorithm. For the SIR epidemic model, we have a state space whose elements are

$$\mathcal{S} = (n_S, n_I, n_R), \quad n = n_S + n_I + n_R.$$

Here,

- n is the number of **individuals** in the population.
- n_S is the number of **susceptible** individuals.
- n_I is the number of **infective** individuals.
- n_R is the number of **recovered** individuals.
- n_C is the number of **cases**, $n_C = n_I + n_R = n - n_S$.

The dynamics on the network corresponds to a continuous time Markov process (S, I, R) with two transitions, shown in the table below.

event	transition	rate
infection	$(n_S, n_I, n_R) \rightarrow (n_S - 1, n_I + 1, n_R)$	$\beta n_S n_I$
recovery	$(n_S, n_I, n_R) \rightarrow (n_S, n_I - 1, n_R + 1)$	γn_I

Underlying Discrete Time Markov Chain

By the Gillespie algorithm, a time-homogeneous pure-jump Markov process consists of two independent parts.

1. The length of time that the process remains in its current state \mathcal{S} , is exponentially distributed with parameter value depending only on the current state, equal to the sum of the rates listed in the above table.
2. The jumps form an underlying time-homogeneous discrete time Markov chain.

For the SIR model, the underlying discrete time Markov chain has two transitions, with probabilities listed in the table below.

event	transition	probability
infection	$(n_S, n_I, n_R) \rightarrow (n_S - 1, n_I + 1, n_R)$	$\beta n_S n_I / (\beta n_S n_I + \gamma n_I)$ $= \beta n_S / (\beta n_S + \gamma)$
recovery	$(n_S, n_I, n_R) \rightarrow (n_S, n_I - 1, n_R + 1)$	$\gamma n_I / (\beta n_S n_I + \gamma n_I)$ $= \gamma / (\beta n_S + \gamma)$

Note that the probabilities in the last column were simplified after assuming $n_I > 0$. Choosing state space variables n_C and n_I , we recast the Markov chain transitions in terms of the total population n and the number of cases n_C , leading to the following table.

event	transition	probability
infection	$(n_C, n_I) \rightarrow (n_C + 1, n_I + 1)$	$\lambda(n_C) = \beta(n - n_C) / (\beta(n - n_C) + \gamma)$
recovery	$(n_C, n_I) \rightarrow (n_C, n_I - 1)$	$1 - \lambda(n_C) = \gamma / (\beta(n - n_C) + \gamma)$

Using the expression for the basic reproduction number, $R_0 = n\beta/\gamma = \beta_P/\gamma$, we can also write

$$\lambda(n_C) = \frac{R_0(n - n_C)/n}{R_0(n - n_C)/n + 1}.$$

Here, $\beta_P = n\beta$ is the population **contact rate**. Since we are assuming that $n_I > 0$ and the infection spreads, we also assume that $R_0 > 1$. Consequently, we can denote the underlying Markov chain by C_j , $j = 0, 1, \dots$ for the total number of cases at the j -th event. Note that C_j is a pure birth chain with a jump up with each new infection.

Cast in this way, we have two parameters for the SIR model, namely β and R_0 . In terms of statistical inference, the ratio that leads to the probabilities $\lambda(n_C)$ shows that the parameter β is **ancillary** to the dynamics of the discrete time Markov chain. We shall learn how this property greatly simplifies inference and allows us to focus on R_0 .

The Distribution of the Number of Infected Individuals

Set

$$\tau_{n_C} = \min\{j; C_j = n_C\}.$$

The goal of this section is to determine the distribution of the number of infected individuals $I_{\tau_{n_C}}$ when the number of cases is known. Then,

$$I_{\tau_{n_C}} = n_c - (\tau_{n_C} - n_c) = 2n_C - \tau_{n_C}$$

since there have been n_c infections in τ_{n_C} steps, and thus $\tau_{n_C} - n_c$ recoveries. This shows that if we can determine the distribution of τ_{n_C} , then we can determine the distribution of $I_{\tau_{n_C}}$. We will first develop an asymptotic approximation of mean, variance, and skewness suitable for larger populations. This will lead to a functional central limit for the number of infections $I_{\tau_{n_C}}$.

Means, Variances, and Skewness

A pure-birth Markov chain remains in a given state m for a geometric number of steps before making the transition to the state $m + 1$. With this in mind, we can write

$$\tau_{n_C} = \sigma_1 + \cdots + \sigma_{n_C-1}$$

as the sum of independent random variables $\sigma_m \sim \text{Geom}_1(\lambda(m))$. Here, the subscript 1 indicates that the the state space is $\{1, 2, \dots\}$ rather than $\{0, 1, 2, \dots\}$. Thus,

$$E\sigma_m = \frac{1}{\lambda(m)} \quad \text{and} \quad \text{Var}(\sigma_m) = \frac{1 - \lambda(m)}{\lambda(m)^2}.$$

Now use the linearity of expectation and the properties of variance for independent random variables to see that

$$\begin{aligned} E\tau_{n_C} &= \sum_{m=1}^{n_C-1} \frac{1}{\lambda(m)} = \sum_{m=1}^{n_C-1} \frac{R_0(n-m)/n + 1}{R_0(n-m)/n} = (n_C - 1) + \frac{n}{R_0} \sum_{m=1}^{n_C-1} \frac{1}{n-m}, \\ \text{Var}(\tau_{n_C}) &= \sum_{m=1}^{n_C-1} \frac{1 - \lambda(m)}{\lambda(m)^2} = \sum_{m=1}^{n_C-1} \frac{1/(R_0(n-m)/n + 1)}{((R_0(n-m)/n)/(R_0(n-m)/n + 1))^2} \\ &= \sum_{m=1}^{n_C-1} \frac{R_0(n-m)/n + 1}{R_0^2(n-m)^2/n^2} = \frac{n}{R_0} \sum_{m=1}^{n_C-1} \frac{1}{n-m} + \frac{n^2}{R_0^2} \sum_{m=1}^{n_C-1} \frac{1}{(n-m)^2}. \end{aligned}$$

Consequently,

$$\begin{aligned} EI_{\tau_{n_C}} &= 2n_C - E\tau_{n_C} = (n_C + 1) - \frac{n}{R_0} \sum_{m=1}^{n_C-1} \frac{1}{n-m}, \\ \text{Var}(I_{\tau_{n_C}}) &= \text{Var}(\tau_{n_C}) = \frac{n}{R_0} \sum_{m=1}^{n_C-1} \frac{1}{n-m} + \frac{n^2}{R_0^2} \sum_{m=1}^{n_C-1} \frac{1}{(n-m)^2}. \end{aligned}$$

The skewness γ_1 of a $\zeta \sim \text{Geom}_1(p)$ random variable is $(2-p)/\sqrt{1-p}$. Thus, the third central moment

$$E(\zeta - 1/p)^3 = \gamma_1 \sigma^3 = \frac{2-p}{(1-p)^{1/2}} \frac{(1-p)^{3/2}}{p^3} = \frac{(2-p)(1-p)}{p^3}.$$

If we write $z_m = R_0(n-m)/n + 1$, then the third central moment of σ_m is

$$\frac{(2 - \lambda(m))(1 - \lambda(m))}{\lambda^3(m)} = \frac{(2 - (z_m - 1)/z_m)(1 - (z_m - 1)/z_m)}{((z_m - 1)/z_m)^3} = \frac{(z_m + 1)z_m}{(z_m - 1)^3}.$$

Thus, the third central moment of τ_{n_C} reads

$$\kappa_{n_C} = \sum_{m=1}^{n_C-1} \frac{(z_m + 1)z_m}{(z_m - 1)^3} = \sum_{m=1}^{n_C-1} \frac{(R_0(n-m)/n + 2)(R_0(n-m)/n + 1)}{(R_0(n-m)/n)^3}.$$

The skewness of τ_{n_C} is $\kappa_{n_C}/\text{Var}(I_{\tau_{n_C}})^{3/2}$.

Asymptotics

The mean, variance, and skewness can be well approximated by an integral. We will consider the circumstance as the infection moves from $n_0 = n c_0$ cases to $n_C = n c$ cases. Set $c_m = m/n$. For the mean,

$$\begin{aligned} \frac{1}{n}(E\tau_{n_C} - E\tau_{n_0}) &= c - c_0 + \frac{1}{R_0} \sum_{m=n c_0}^{n c-1} \frac{1}{1 - c_m} \frac{1}{n} \\ &\rightarrow c - c_0 + \frac{1}{R_0} \int_{c_0}^c \frac{1}{1 - q} dq = c - c_0 + \frac{1}{R_0} \ln \left(\frac{1 - c_0}{1 - c} \right) \quad \text{as } n \rightarrow \infty. \end{aligned}$$

Thus,

$$\frac{1}{n}(EI_{\tau_{n_C}} - EI_{\tau_{n_0}}) \rightarrow c - c_0 - \frac{1}{R_0} \ln \left(\frac{1 - c_0}{1 - c} \right) \quad \text{as } n \rightarrow \infty.$$

For the variance,

$$\begin{aligned} \frac{1}{n}(\text{Var}(\tau_{n_C}) - \text{Var}(\tau_{n_0})) &= \frac{1}{R_0} \sum_{m=n c_0}^{n c-1} \frac{1}{1 - c_m} \frac{1}{n} + \frac{1}{R_0^2} \sum_{m=n c_0}^{n c-1} \frac{1}{(1 - c_m)^2} \frac{1}{n} \\ &\rightarrow \frac{1}{R_0} \int_{c_0}^c \frac{1}{1 - q} dq + \frac{1}{R_0^2} \int_{c_0}^c \frac{1}{(1 - q)^2} dq \quad \text{as } n \rightarrow \infty \\ &= \frac{1}{R_0} \ln \left(\frac{1 - c_0}{1 - c} \right) + \frac{1}{R_0^2} \frac{c - c_0}{(1 - c)(1 - c_0)}. \end{aligned}$$

To compute the skewness, we use the limit as $n \rightarrow \infty$ of Riemann sums for the third central moment

$$\begin{aligned} \frac{\kappa_{n_C}}{n} - \frac{\kappa_{n_{C_0}}}{n} &= \sum_{m=n c_0}^{n c-1} \frac{(R_0(1 - c_m) + 2)(R_0(1 - c_m) + 1)}{(R_0(1 - c_m))^3} \frac{1}{n} \\ &\rightarrow \int_{c_0}^c \frac{(R_0(1 - q) + 2)(R_0(1 - q) + 1)}{(R_0(1 - q))^3} dq \quad \text{as } n \rightarrow \infty \\ &= \int_{c_0}^c \left(\frac{1}{R_0(1 - q)} + \frac{3}{R_0^2(1 - q)^2} + \frac{2}{R_0^3(1 - q)^3} \right) dq \\ &= \frac{1}{R_0} \ln \left(\frac{1 - c_0}{1 - c} \right) + \frac{3}{R_0^2} \frac{c - c_0}{(1 - c)(1 - c_0)} + \frac{1}{R_0^3} \frac{(c - c_0)(2 - (c + c_0))}{(1 - c)^2(1 - c_0)^2}. \end{aligned}$$

Functional Central Limit Theorems

We can turn the calculations above into a functional central limit theorem. To start, define

$$\bar{I}_c = \frac{1}{n} I_{\tau_{n_C}}, \quad \bar{\tau}_c = \frac{1}{n} \tau_{n_C}.$$

Due to the fact that they are derived from sums of independent geometric random variables, both \bar{I}_c and $\bar{\tau}_c$ have independent increments. For example, define \mathcal{F}_c to be the σ -algebra generated by $\{C_j; j \leq \tau_{n_c}\}$. Then for $c_0 < c_1$, $\bar{\tau}_{c_1} - \bar{\tau}_{c_0}$ and \mathcal{F}_{c_0} are independent and by the basic properties of conditional expectation

$$E[\bar{\tau}_{c_1} - \bar{\tau}_{c_0} | \mathcal{F}_{c_0}] = E[\bar{\tau}_{c_1} - \bar{\tau}_{c_0}] = E\bar{\tau}_{c_1} - E\bar{\tau}_{c_0}.$$

Rearranging terms,

$$E[\bar{\tau}_{c_1} - E\bar{\tau}_{c_1} | \mathcal{F}_{c_0}] = \bar{\tau}_{c_0} - E\bar{\tau}_{c_0},$$

where we have used $E[E\bar{\tau}_{c_1} | \mathcal{F}_{c_0}] = E\bar{\tau}_{c_1}$ and $E[\bar{\tau}_{c_0} | \mathcal{F}_{c_0}] = \bar{\tau}_{c_0}$. Next, define

$$M_c^n = \sqrt{n}(\bar{I}_c - E\bar{I}_c) = -\sqrt{n}(\bar{\tau}_c - E\bar{\tau}_c).$$

Then,

$$E[M_{c_1}^n | \mathcal{F}_{c_0}] = M_{c_0}^n,$$

showing that M_c^n is a mean zero martingale. Continuing, set

$$A_c^n = n\text{Var}(\bar{I}_c) = n\text{Var}(\bar{\tau}_c) = \text{Var}(M_c^n).$$

Using the mean zero and independent increments properties again, we find

$$E[(M_{c_1}^n - M_{c_0}^n)^2 | \mathcal{F}_{c_0}] = \text{Var}(M_{c_1}^n - M_{c_0}^n | \mathcal{F}_{c_0}) = \text{Var}(M_{c_1}^n - M_{c_0}^n) = A_{c_1}^n - A_{c_0}^n.$$

Also,

$$E[(M_{c_1}^n - M_{c_0}^n)^2 | \mathcal{F}_{c_0}] = E[(M_{c_1}^n)^2 | \mathcal{F}_{c_0}] - 2M_{c_0}^n E[M_{c_1}^n | \mathcal{F}_{c_0}] + (M_{c_0}^n)^2 = E[(M_{c_1}^n)^2 | \mathcal{F}_{c_0}] - (M_{c_0}^n)^2.$$

Combining,

$$E[(M_{c_1}^n)^2 | \mathcal{F}_{c_0}] - (M_{c_0}^n)^2 = A_{c_1}^n - A_{c_0}^n, \quad \text{and} \quad E[(M_{c_1}^n)^2 - A_{c_1}^n | \mathcal{F}_{c_0}] = (M_{c_0}^n)^2 - A_{c_0}^n.$$

Showing that

$$(M_c^n)^2 - A_c^n$$

is also a martingale.

The martingale central limit theorem has three ingredients:

1. A sequence of martingales, here the sequence of stochastic processes M_c^n .
2. A sequence of positive processes A_c^n that compensate for $(M_c^n)^2$ so that $(M_c^n)^2 - A_c^n$ is a martingale.
3. A_c^n converges to a deterministic function continuous in c . Here $A_c^n \rightarrow \sigma_I^2(c)$ as $n \rightarrow \infty$, where

$$\sigma_I^2(c) = -\frac{1}{R_0} \ln(1-c) + \frac{1}{R_0^2} \frac{c}{(1-c)},$$

and we have set $c_0 = 0$ in the asymptotic expansions derived in the previous section, to obtain an expression in terms of c only.

If 1, 2, and 3 hold, then the sequence of martingales converges to a mean-zero independent increments Gaussian process. (See [14] Section 7.1.) We, now, state the result formally.

Theorem 1. M_c^n converges in distribution as $n \rightarrow \infty$ to a continuous Gaussian process with independent increments with variance function $\sigma_I^2(c)$ and mean zero.

Consequently, the mean of the scaled infected satisfies

$$E\bar{I}_c \simeq m_I(c) = c + \frac{1}{R_0} \ln(1 - c)$$

and the variance

$$\text{Var}(\bar{I}_c) \simeq \frac{1}{n} \sigma_I^2(c),$$

with equality in the limit as $n \rightarrow \infty$.

We now turn to the scaled stochastic incidence for population n , which we define as

$$\frac{\mathcal{I}}{n} = \mathcal{I}_n = (\beta n) \bar{I}_c (1 - c), \quad \mathcal{I} = \beta n_I n_S.$$

Note that as $n \rightarrow \infty$, the population contact rate $\beta_P = \beta n$ remains constant for fixed $R_0 = (\beta n)/\gamma = \beta_P/\gamma$. A similar central limit theorem applies to \mathcal{I}_n . The mean scaled incidence rate is obtained from the scaled number of infections

$$G_I(c) = (\beta n) m_I(c) (1 - c),$$

as stated below.

Corollary 2. *The scaled limit of \mathcal{I}_n converges to an independent increments Gaussian process, of mean*

$$G_I(c) = (\beta n) \left(c + \frac{1}{R_0} \ln(1 - c) \right) (1 - c)$$

and variance $\frac{1}{n} \sigma_G^2(c)$, where

$$\sigma_G^2(c) = (\beta n)^2 \sigma_I^2(c) (1 - c)^2 = \beta_P^2 \left(-\frac{1}{R_0} \ln(1 - c) + \frac{1}{R_0^2} \frac{c}{(1 - c)} \right) (1 - c)^2.$$

To obtain a formula for the variance of an increment, first note that for $c > c_0$, \bar{I}_c and $\bar{I}_c - \bar{I}_{c_0}$ are independent. Thus,

$$0 = \text{Cov}(\bar{I}_c - \bar{I}_{c_0}, \bar{I}_{c_0}) = \text{Cov}(\bar{I}_c, \bar{I}_{c_0}) - \text{Var}(\bar{I}_{c_0})$$

and

$$\lim_{n \rightarrow \infty} n \text{Cov}(\bar{I}_c, \bar{I}_{c_0}) = \lim_{n \rightarrow \infty} n \text{Var}(\bar{I}_{c_0}) = \sigma_I^2(c_0).$$

Continuing,

$$\begin{aligned}
& n\text{Var}(\beta\bar{I}_c(1-c) - \beta\bar{I}_{c_0}(1-c_0)) \\
&= n\beta^2 \left((1-c)^2\text{Var}(\bar{I}_c) - 2(1-c)(1-c_0)\text{Cov}(\bar{I}_c, \bar{I}_{c_0}) + (1-c_0)^2\text{Var}(\bar{I}_{c_0}) \right) \\
&\rightarrow \beta^2 \left((1-c)^2\sigma_I^2(c) - 2(1-c)(1-c_0)\sigma_I^2(c_0) + (1-c_0)^2\sigma_I^2(c_0) \right) \quad \text{as } n \rightarrow \infty \\
&= \beta^2 \left((1-c)^2\sigma_I^2(c) - (1-c_0)(2(1-c) - (1-c_0))\sigma_I^2(c_0) \right) \\
&= \beta^2 \left((1-c)^2\sigma_I^2(c) + (1-c_0)(2c - c_0 - 1)\sigma_I^2(c_0) \right) = \sigma_G^2(c_0, c)/n.
\end{aligned}$$

We should also remark that we can determine the number of recovered at the stopping time τ_{n_C} by noting that

$$\begin{aligned}
R_{\tau_{n_C}} - R_{\tau_{n_0}} &= (\tau_{n_C} - \tau_{n_0}) - (n_C - n_0) = -(I_{\tau_{n_C}} - I_{\tau_{n_0}}) + (n_C - n_0) \\
\frac{1}{n}(R_{\tau_{n_C}} - R_{\tau_{n_0}}) &= -\frac{1}{n}(I_{\tau_{n_C}} - I_{\tau_{n_0}}) + (c - c_0) = -(\bar{I}_c - \bar{I}_{c_0}) + (c - c_0).
\end{aligned}$$

Corollary 3. *The scaled limit of R converges to an independent increments Gaussian process. The mean of the increment from c_0 to c is*

$$m_R(c) - m_R(c_0) = \frac{1}{R_0} \ln \left(\frac{1-c_0}{1-c} \right).$$

The variance satisfies $\sigma_R^2(c) = \sigma_I^2(c)$. The limiting processes for I and R have correlation -1.

Final Population Size and Peak Incidence for an Epidemic

Important properties of a disease outbreak are given at critical values c_* for the fraction of cases. Two particularly relevant examples of c_* are

1. c_\wedge , the *fraction infected at peak incidence* when $G'_I(c_\wedge) = 0$, and
2. c_∞ , the *total fraction of cases* when $m_I(c_\infty) = 0$.

For the first,

$$\begin{aligned}
0 = G'_I(c_\wedge) &= (\beta n) \left((m'_I(c_\wedge)(1-c_\wedge) - m_I(c_\wedge)) \right) \\
&= (\beta n) \left(\left(\left(1 - \frac{1}{R_0} \frac{1}{1-c_\wedge} \right) (1-c_\wedge) - \left(c_\wedge + \frac{1}{R_0} \ln(1-c_\wedge) \right) \right) \right) \\
&= (\beta n) \left(\left(\left((1-c_\wedge) - \frac{1}{R_0} \right) - \left(c_\wedge + \frac{1}{R_0} \ln(1-c_\wedge) \right) \right) \right) \\
&= (\beta n) \left(1 - 2c_\wedge - \frac{1}{R_0} (1 + \ln(1-c_\wedge)) \right) \\
c_\wedge &= \frac{-1}{2R_0} (1 + \ln(1-c_\wedge)) + \frac{1}{2},
\end{aligned}$$

which can be solved numerically. Returning to the functional central limit theorem of scaled incidence, the standard deviation of the scaled incidence \mathcal{I}_n at c_\wedge is

$$(\beta n)\sigma_\wedge/\sqrt{n}, \quad \text{where we define} \quad \sigma_\wedge = \sigma_I(c_\wedge)(1 - c_\wedge).$$

The second requires the variant of the delta method applied to hitting times. (See [14], Section 11.4.) This approach uses propagation of error to give a valuable extension of the central limit theorem. Here, we define

$$\hat{c}_\infty = \inf\{c > 0; \bar{I}_c = 0\}.$$

Then, because $\bar{I}_c \rightarrow m_I(c)$ as $n \rightarrow \infty$, we have $\hat{c}_\infty \rightarrow c_\infty$. By the central limit theorem (Theorem 1 of the previous section),

$$\sqrt{n}(\bar{I}_{\hat{c}_\infty} - m_I(\hat{c}_\infty)) \rightarrow W$$

where $W \sim N(0, \sigma_I^2(c_\infty))$, a normal random variable with mean 0 and variance $\sigma_I^2(c_\infty)$. Next, recall that $m_I(c_\infty) = \bar{I}_{\hat{c}_\infty} = 0$, thus

$$\sqrt{n}(\bar{I}_{\hat{c}_\infty} - m_I(\hat{c}_\infty)) = \sqrt{n}(m_I(c_\infty) - m_I(\hat{c}_\infty)) \simeq \sqrt{n}m'_I(c_\infty)(c_\infty - \hat{c}_\infty)$$

Consequently, \hat{c}_∞ is approximately normally distributed, with mean c_∞ and standard deviation

$$\sigma(\hat{c}_\infty) \approx \frac{1}{|m'(c_\infty)|} \frac{\sigma_I(c_\infty)}{\sqrt{n}} = \frac{\sigma_\infty}{\sqrt{n}}.$$

Thus, the standard deviation is multiplied by a propagation of error which is inversely proportional to the slope of $m_I(c_\infty)$. The error is expanded when the slope is shallow and contracted when the slope is steep.

For c_∞ , we solve implicitly.

$$0 = m_I(c_\infty) = c_\infty + \frac{1}{R_0} \ln(1 - c_\infty), \quad \text{i.e.} \quad c_\infty = -\frac{1}{R_0} \ln(1 - c_\infty).$$

Now substitute into the variance formula.

$$\sigma_I^2(c_\infty) = -\frac{1}{R_0} \ln(1 - c_\infty) + \frac{1}{R_0^2} \frac{c_\infty}{1 - c_\infty} = c_\infty + \frac{1}{R_0^2} \frac{c_\infty}{1 - c_\infty}.$$

The derivative

$$m'_I(c_\infty) = 1 - \frac{1}{R_0} \frac{1}{1 - c_\infty}$$

leads to

$$\begin{aligned} \frac{\sigma_I^2(c_\infty)}{m'_I(c_\infty)^2} &= \frac{c_\infty + \frac{1}{R_0^2} \frac{c_\infty}{1 - c_\infty}}{\left(1 - \frac{1}{R_0} \frac{1}{1 - c_\infty}\right)^2} = \frac{R_0^2 c_\infty (1 - c_\infty)^2 + c_\infty (1 - c_\infty)}{(R_0(1 - c_\infty) - 1)^2} \\ &= \frac{c_\infty (1 - c_\infty) (R_0^2 (1 - c_\infty) + 1)}{(R_0(1 - c_\infty) - 1)^2}. \end{aligned}$$

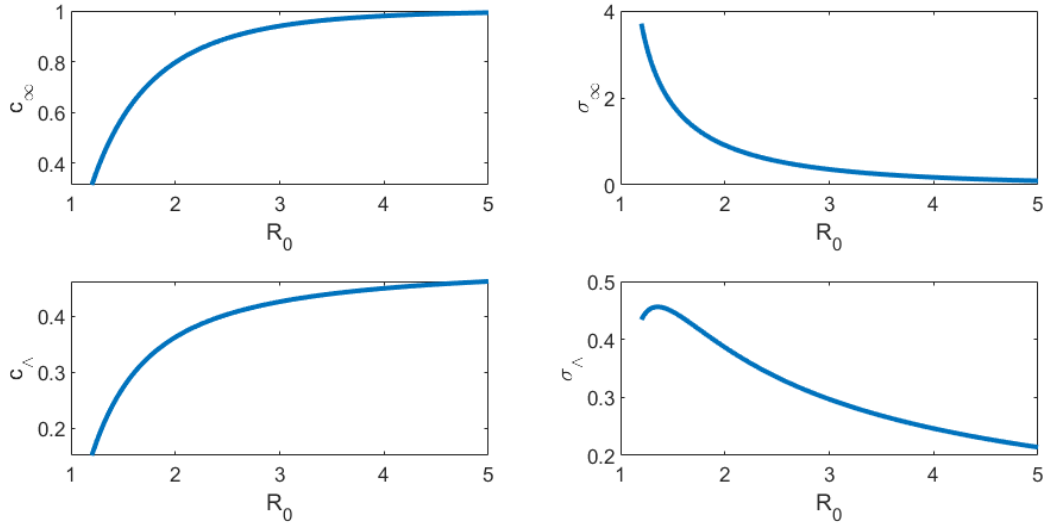


Figure 4: **Top row, left:** Values for the mean $\mu_{\hat{c}_\infty} = c_\infty$, the fraction of population that eventually become cases. **Bottom row, left:** The expected fraction of cases at peak infection $\mu_{\hat{c}_\wedge} = c_\wedge$. **Top row, right:** For a population of size n , the standard deviation for \hat{c}_∞ is σ_∞/\sqrt{n} . **Bottom row, right:** The standard deviation of \mathcal{I}_n at mean peak incidence is $(\beta n)\sigma_\wedge/\sqrt{n}$.

Now take the square root and substitute into the formula for $\sigma(\hat{c}_\infty)$.

The central limit theorem for c_∞ has been known for some time (see [16, 17]). As the graphs associated to c_∞ show, the course of the pandemic looks more and more deterministic as R_0 grows, with an increase in cases and reduction in the standard deviation σ_∞ . The peak incidence increases with R_0 from 0.152 to 0.462 as R_0 increases from 1.2 to 5.0. The standard deviation σ_\wedge decreases with R_0 for $R_0 > 1.5$.

References

- [1] D. Morens, A. Fauci, *PLoS Pathog* **9**, e1003467 (2013).
- [2] C. E. Walters, M. M. Meslé, I. M. Hall, *Epidemics* **25**, 1 (2018).
- [3] J. Lega, H. E. Brown, *Epidemics* **17**, 19 (2016).
- [4] J. Lega, *Parameter Estimation from ICC Curves*, to appear in *J. Biol. Dyn.* (2021).
url=<https://arxiv.org/abs/2005.08134>.
- [5] State of Arizona Executive Order 2020-09, *Limiting The Operations Of Certain Businesses To Slow The Spread Of COVID-19*. March 19, 2020.
url=<https://azgovernor.gov/executive-orders>.
- [6] State of Arizona Executive Order 2020-18, *Stay Home, Stay Healthy, Stay Connected*.
March 30, 2020. url=<https://azgovernor.gov/executive-orders>.
- [7] State of Arizona Executive Order 2020-33, *Returning Stronger. Amending the Stay Home, Stay Healthy, Stay Connected Order*. April 29, 2020.
url=<https://azgovernor.gov/executive-orders>.
- [8] State of Arizona Executive Order 2020-34, *Building On COVID-19 Successes*. May 4, 2020. url=<https://azgovernor.gov/executive-orders>.
- [9] State of Arizona Executive Order 2020-36, *Stay Healthy, Return Smarter, Return Stronger*. May 12, 2020. url=<https://azgovernor.gov/executive-orders>.
- [10] M. Bartlett, *Journal of the Royal Statistical Society. Series B (Methodological)* **11**, 211 (1949).
- [11] L. Breiman, *Probability*, Addison-Wesley series in statistics (Addison-Wesley Publishing Company, 1968).
- [12] D. T. Gillespie, *Journal of Computational Physics* **22**, 403 (1976).
- [13] A. F. Bartholomay, *The bulletin of mathematical biophysics* **20**, 97 (1958).
- [14] S. N. Ethier, T. G. Kurtz, *Markov processes: characterization and convergence*, vol. 282 (John Wiley & Sons, 2009).
- [15] T. Sellke, *Journal of Applied Probability* pp. 390–394 (1983).
- [16] G. Scalia-Tomba, *Advances in Applied Probability* **17**, 477 (1985).
- [17] G. Scalia-Tomba, *Stochastic Processes in Epidemic Theory* (Springer Berlin Heidelberg, 1990), pp. 189–196.

- [18] M. Ghosh, N. Reid, D. Fraser, *Statistica Sinica* pp. 1309–1332 (2010).
- [19] J. L. Juul, K. Græsbøll, L. E. Christiansen, S. Lehmann, *Nature Physics* **17**, 5 (2020).
- [20] W. O. Kermack, A. G. McKendrick, *Proceedings of the Royal Society of London. Series A, Containing Papers of a Mathematical and Physical Character* **115**, 700 (1927).
- [21] B. Rudis, *cdcfluview: Retrieve Flu Season Data from the United States Centers for Disease Control and Prevention ('CDC') 'FluView' Portal* (2020). R package version 0.9.2.
- [22] The COVID Tracking Project at *The Atlantic*. All data and content are available under a CC BY-NC-4.0 license (<https://covidtracking.com/license>). Data were downloaded through the project API: <https://covidtracking.com/data/api>.